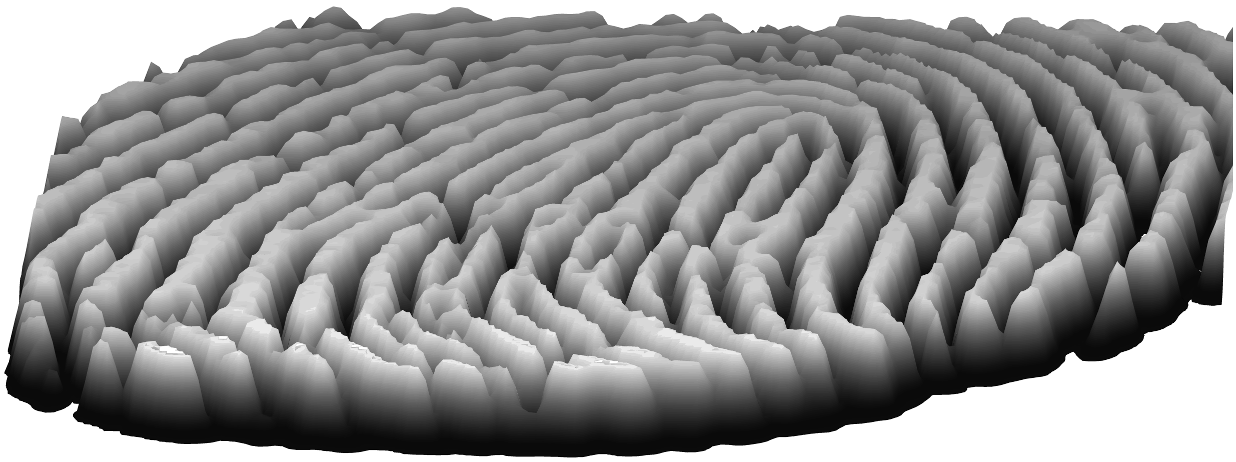

ASIC System Design Considerations for Under-glass Fingerprint Sensors

An investigation into system performance using capacitive technology

Master's thesis in Embedded Electronic System Design

JOHANNES ARVIDSSON
RASMUS SÖDERSTRÖM OLSSON

Department of Computer Science and Engineering
CHALMERS UNIVERSITY OF TECHNOLOGY
UNIVERSITY OF GOTHENBURG
Gothenburg, Sweden 2018

ASIC System Design Considerations for Under-glass Fingerprint Sensors

An investigation into system performance using capacitive technology

JOHANNES ARVIDSSON
RASMUS SÖDERSTRÖM OLSSON

Department of Computer Science and Engineering
Chalmers University of Technology
University of Gothenburg
Gothenburg, Sweden 2018

ASIC System Design Considerations for Under-glass Fingerprint Sensors
An investigation into system performance using capacitive technology
JOHANNES ARVIDSSON
RASMUS SÖDERSTRÖM OLSSON

Supervisor: Daniel Andersson, Fingerprint Cards AB, ASIC team
Supervisor: Lars Svensson, Department of Computer Science and Engineering
Examiner: Per Larsson-Ederfors, Department of Computer Science and Engineering

Department of Computer Science and Engineering
Chalmers University of Technology
University of Gothenburg
SE-412 96 Gothenburg
Telephone +46 31 772 1000

Cover: Topology map of a fingerprint captured on a capacitive sensor.

Typeset in LaTeX
Gothenburg, Sweden 2018

ASIC System Design Considerations for Under-glass Fingerprint Sensors
An investigation into system performance using capacitive technology
JOHANNES ARVIDSSON
RASMUS SÖDERSTRÖM OLSSON
Department of Computer Science and Engineering
Chalmers University of Technology
University of Gothenburg

Abstract

Placing a fingerprint sensor under thick glass puts heavy performance requirements on the mixed signal path in the ASIC that constitutes the sensor. This thesis will explore and explain different effects that can be observed when the distance between a finger and a capacitive sensor is increased. We will motivate why these effects are detrimental to performance and try to combat them with proposed system-level design changes. Fast-capture of fingerprint images have been used to characterize contrast over time; the time behavior of contrast could not be used to circumvent detrimental effects of using thick glass. Instead, focus has been placed on reducing noise using extensive multisampling, using a dynamic sample count based on finger movement, with positive results. A reduction in pixel noise power of approximately 50% compared to a currently used sensor design has been achieved within the same sampling time frame.

Keywords: ASIC, System Design, Fingerprint, Sensors, Thick Glass.

Acknowledgements

We would like to give the sincerest of thanks to Lars Svensson, our supervisor at Chalmers. He proved, time and again, that he is invaluable for the students with his humorous trademark, calming yet motivational words and abundant technical knowledge.

An additional thanks to our supervisor Daniel Andersson at FPC, with his knowledge in different tools and contacts within the company made this thesis viable. He also made us dive into novel fields with renewed energy and constantly pushed for new discoveries.

Lastly, we would like to thank all who provided feedback and insight, answered our questions on lab equipment, software, system design and algorithms, you truly made us see what it takes to be a role model engineer.

Johannes Arvidsson and Rasmus Söderström Olsson

Gothenburg, June 2018

Nomenclature

ADC: Analog-to-Digital Converter, converts analog signals to digital signals.

ASIC: Application-Specific Integrated Circuit, in this thesis a mixed signal device, often called “sensor”.

FIFO: First In, First Out, a data structure using the the first come, first serve principle.

FPC: Fingerprint Cards AB.

Host: The system that the fingerprints sensors sends the data to, often a CPU situated in a PC or smartphone.

NRE cost: Non-recurring engineering cost, the one-time cost to design, develop and test a new product.

Ridge: A high section of a fingerprint.

SNR: Signal to Noise Ratio, usually expressed in decibel (dB).

SPI: Serial Peripheral Interface bus, a synchronous serial communication interface specification often used for short distance communication.

Stack-up: A group-term that addresses all materials between the fingerprint sensor ASIC and a finger. This could include overmold plastic, different glues, and glass or ceramics.

Valley: A low section of a fingerprint.

Contents

1

Introduction

Capacitive sensing structures are widely used as a means of identifying fingerprints. The current main application for this technology is the mobile phone industry with some upcoming markets such as *smart cards* and *automotive* [1]. Cosmetic design goals in the smartphone industry call for sensors to be placed under glass and this puts heavy performance requirements on the fingerprint sensors.

1.1 Background

The smartphone industry has been longing for high-performing fingerprint sensors that are capable of fingerprint detection whilst being mounted under the display glass. Several different approaches such as optical, thermal, ultrasonic, pressure, capacitive, and sensor fusion variants exist [2][3]. Some of the technologies such as thermal and the sensor fusion variants have not been implemented in the smartphone industry and infra-red is currently not being pursued by any of the major companies in the market. Optical sensors have struggled to gain design wins in smartphones due to their complexity and cost. They remain an alternative for defense and governmental applications despite the fact that they are more easily spoofed than capacitive sensors [4]. Ultrasonic sensors have claimed robustness to particularly difficult conditions regarding the materials between the sensor and the finger, hereafter referred to as the stack-up, that might render them successful in under-glass mounting. However, only two smartphone models utilizing an ultrasonic sensor have been announced since 2016 and none of them actually made it to the market [5].

Asahi Glass announced a special manufacturing process in early 2016 which enables mounting of capacitive fingerprint sensors under glass by making the display glass thinner at the sensor [6]. This process is expensive, and a fingerprint sensor which does not need the special glass from Asahi is clearly favorable to one that does. Today this is still the only option for capacitive sensors mounted under glass.

1.2 Fingerprint Cards and Supply Chain

Fingerprint Cards AB (FPC) is a global leader in biometrics but foremost in capacitive fingerprint sensors. Their sensors are mainly targeted towards the mobile phone industry where they provide user authentication. The sensors are designed by FPC and manufactured as an Application Specific Integrated Circuit (ASIC) in the form of silicon wafers, which are then sold to module houses for further packaging and module manufacturing. The final customer is the mobile phone manufacturers which integrate the modules into their products.

1.3 Problem Formulation

It is well known in industry that thick glass between a finger and the sensor drastically degrades signal levels and noise performance in capacitive fingerprint sensors. Phone designers are pushing for thicker glass and sensor designers are desperately trying to comply. This thesis will explore and explain different effects that can be observed when the distance between a finger and a capacitive sensor is increased. We will motivate why these effects are detrimental to performance and lastly try to combat them with proposed system-level design changes. The aim is to provide solutions which make the capacitive fingerprint sensor less vulnerable to applications with thick stack-ups.

With this, a thorough investigation of the time behavior of a finger is proposed. This investigation should reveal if there are favorable timings in which to capture the fingerprint image to maximize its signal strength. Furthermore, an investigation of the noise performance should be conducted to find possible improvements.

A finger compresses when applying force; this decreases the height difference between a ridge and valley over time [7]. The compression results in that there is significantly more information in an image if taken when the finger is pressed lightly against the sensor, as it would early in the unlocking process. The effects of compression could result in significantly more information in an image if it is taken when the finger is pressed lightly against the sensor, as it would be early in the authentication process. To find this information, the sensor will need the capability to take images at a specific time. If this time is early, the sensor would also have to be fast in reacting to the presence of a finger and supplying an image. Current sensors do not adhere to a set timing scheme and do not fully control the time of capture, making them unable to exploit any optimal times of capture.

The way that a finger spreads out over the sensor when pressed down may also be of interest since the periphery of finger has less pressure on the sensor, i.e. potentially more information, see figure 1.1. To dynamically take smaller sub-images of only the interesting part of the finger might enable the speed required to capture this information.

Figure 1.1: Sketch of how a capacitive fingerprint sensor might interpret a finger being pressed down, with a growing covered area, but also some saturation in the middle of the fingerprint where the finger is being pressed down harder.

1.4 Goals and Challenges

Based on an analysis of the behavior of fingerprint capturing in relation to FPC's state-of-the art sensors, the goal of this project is to find feasible design approaches that can increase biometric performance in applications with thick glass. To achieve this two approaches are considered: understanding finger time behavior to maximize the input signal and improve the noise performance of the system.

Contrast is used as an evaluation metric in the investigation of finger time behavior. Herein contrast is defined as the average difference in pixel value between a ridge (high part) or a valley (low part) of a captured fingerprint image [1]. Contrast is correlated to the measured capacitance difference from ridge to valley, which in turn is correlated to the height difference between a ridge and a valley. Contrast is also a figure of merit in biometric performance; it's easier to identify a fingerprint if the contrast is high. Thus, by looking at contrast for a given sensor setup, we can gauge the height difference of the finger in the captured image and subsequently evaluate the performance of the setup.

To increase the sensor performance we will have to improve the image readout sequence to enable the ASIC to find the information of interest at a sufficient speed. Our project is not required to deliver a complete and implementable design. However, challenges such as those mentioned below still pose some interesting perspectives. We aim to confine our solution to be within reason with respect to these challenges.

- ASIC manufacturing cost

[1] A more thorough definition can be found in section 3.2.

- ASIC power consumption
- Security
- Delay from touch to authentication
- Limited design changes (NRE costs)

1.5 Delimitations

Some areas, while closely related to our goals, cannot or will not be examined during this thesis work. The work is carried out using resources available at Fingerprint Cards AB and the results are therefore not universally applicable on any fingerprint sensor. The algorithm used in the company will not be investigated and consequently not the direct biometric performance of any changes to the design. The technology base for proposed design changes is the capacitive sensing structure described in sections 1.3 and 3.1. A 30 credit thesis work is also limited to a 20 week time span.

2

Theory

This chapter aims to supply the theoretical background required to understand the technical concepts that are discussed in this report. First, capacitive fingerprint sensing is described on a conceptual level; herein the reasons for the diminishing signal levels following thick glass are also explained. A different effect which makes thick glass difficult to use is also explained when looking at the electromagnetic behavior of a sensor set-up in greater detail, namely the point-spread effect. Furthermore some technical concepts are introduced, such as the charge amplifier, which is a fundamental block for capacitive sensing, as well as a description of different noise sources.

2.1 Capacitive Fingerprint Sensing

The capacitive sensing structure relies on the capacitive coupling between the finger and an array of metal plates, from now on referred to as pixel plates, within the sensor as described in figure 2.1. The signal of interest is the difference in capacitance of a plate under a ridge compared to a plate under a valley. The sensor measures capacitance on the pixel plates by producing a voltage change, ΔV across the capacitance, either by changing the potential of the finger or the sensor, and subsequently measures the produced charge change ΔQ on the pixel plate using a charge amplifier. This charge change relates to the capacitance according to equation 2.1.

$$\Delta Q = C \cdot \Delta V \tag{2.1}$$

A simplified model of the signal behavior of this capacitive sensor setup is described in equation 2.2 with regards to pixel area, relative permittivity, glass thickness, and valley depth. Here the pixel plates, and the projected finger segment above them, are assumed to be isolated elements, i.e. no cross-coupling occurs. The relative permittivity of the air in a valley is assumed to be 1 to simplify the expression.

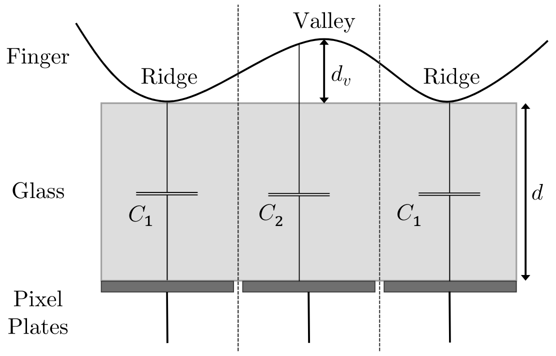

Figure 2.1: Geometric model of a capacitive sensor under glass.

$$C_{signal} = C_1 - C_2 = \varepsilon_0\varepsilon_r\left(\frac{A}{d} - \frac{A}{d + d_v\varepsilon_r}\right) = \varepsilon_0\varepsilon_r^2 A\frac{d_v}{d^2 + d_v d\varepsilon_r}\ [\mathrm{F}] \tag{2.2}$$

The pixel area, A, is restricted by the resolution required in an image to enable the identification of a fingerprint. The limit is about 250 to 300 pixels per inch for detection algorithms to work [2]. However, industry standards such as the ISO-19794-4:2011 and FBI EFTS v7.1 require a minimum of 500 pixels per inch [8][9]. All of Fingerprint Cards sensors adhere to these standards with a pixel area of 50µm×50µm, resulting in 508 pixels per inch [10].

The relative dielectric constant ε_r also has limits, mainly due to cost, since the entire screen glass will have to be made of this dielectric. Expected values range from about 7 for normal glass [11], to about 11.5 for expensive sapphire glass [12][13]. The height difference between a ridge and a valley, d_v, is nominally about 75µm-200µm [14]. It also varies with time and pressure as described in section 1.3.

Figure 2.2 plots the behavior of C_{signal} with regards to glass thickness, d, for different dielectrics, ε_r, and valley depths, d_v. It is observed that major signal degradation occurs with thicker glass and that careful consideration to system parameters must be taken into account when glass thickness is increased.

It should be noted that equation 2.2 is based on a number of assumptions which will not hold in reality, but it is mainly used to illustrate the dependent nature of capacitance difference on stack-up thickness. The equation is based on the model of a simple parallel plate capacitor, which assumes the finger to be as large as the pixel plate, i.e the only contribution to the capacitance comes from directly above the plate. Gauss's Law is used to calculate the capacitance which assumes that the parallel plates are large and have uniformly distributed charge which is equal and opposite. It also assumes that the electric field is uniform between the plates [15]. These are conventionally good assumptions, but are violated when looking at more than one pair of conducting bodies in the same space [16]. To further describe the behavior of the capacitance all pixel plates and their corresponding finger segments will have to

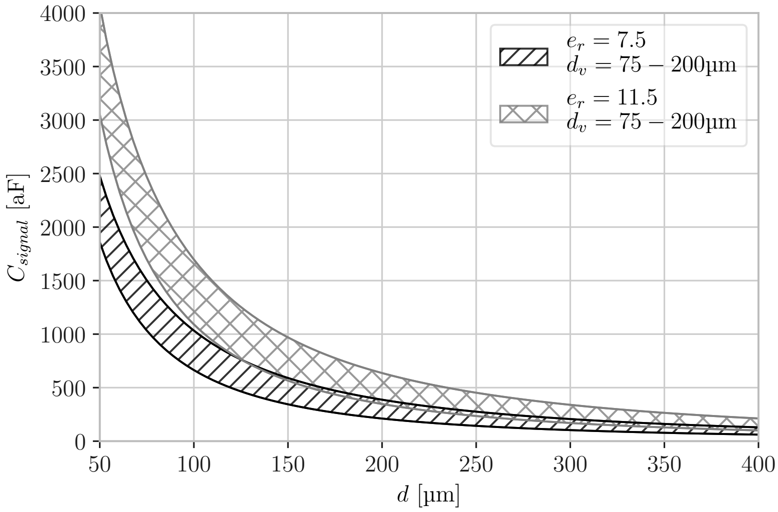

Figure 2.2: Signal levels for different glass thicknesses. C_{signal} is heavily dependent on glass thickness d.

be taken into account simultaneously to build a more accurate finger-sensor model. This is further described in section 2.2.

2.2 Electrostatic Behavior

To more accurately describe the electromagnetic behavior between the sensor and a finger, the model will be discretized and described as a set of conductors, where each pixel plate and finger segment projected by the pixel plates is its own individual conductor. In this set each conductor exhibits a capacitive coupling to all other conductors, as well as to some ground plane, assumed at infinite distance. To draw this would be increasingly cluttered, even for a few number of conductors, but figure 2.3 describes the model described in figure 2.1 where all capacitive couplings have been drawn for the middle pixel plate.

2.2.1 Coefficients of Capacitance

The coefficients of capacitance, also known as the Maxwell capacitance matrix, describes the relation between voltage and charge for a general set of conductors according to equation 2.3 [16]. The Maxwell matrix is often used in presenting the result from electric-field solvers [17].

$$\mathbf{Q} = \mathbf{C} \cdot \mathbf{V} \tag{2.3}$$

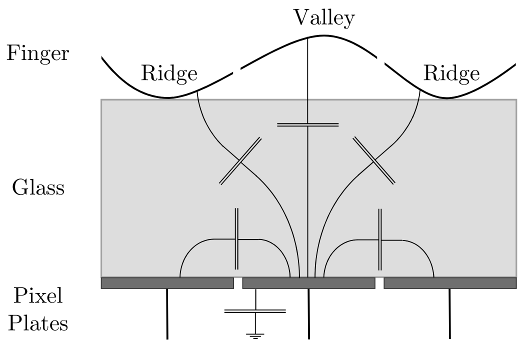

Figure 2.3: All capacitive couplings explicitly drawn for the middle pixel plate.

Here, **C** is the Maxwell matrix, **Q** is the charge vector, and **V** is the potential vector. The Maxwell matrix can be derived from the capacitances in a physical system, independent on the charge state of the circuit.

In figure 2.4, an example is made based on a set of four ideal conductors described together with their mutual capacitances as well as the capacitances towards infinity.

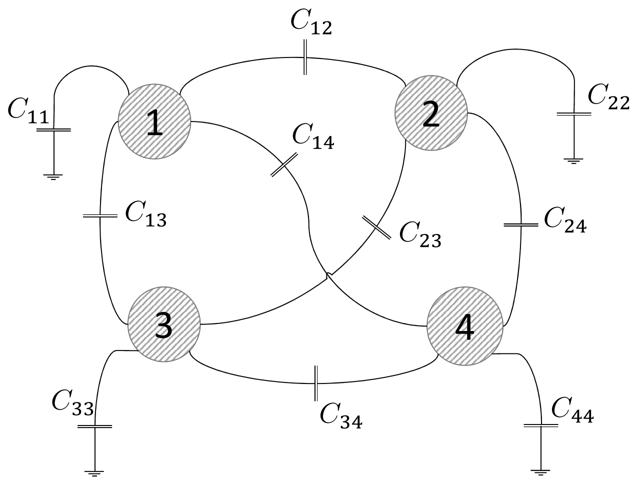

Figure 2.4: Mutual and auto capacitances for four conductors.

The capacitive couplings for *conductor 1* can therefore be described by equation 2.4.

$$\begin{aligned} Q_1 &= C_{11} \cdot V_1 + C_{12} \cdot (V_1 - V_2) + C_{13} \cdot (V_1 - V_3) + C_{14} \cdot (V_1 - V_4) \\ &= (C_{11} + C_{12} + C_{13} + C_{14}) \cdot V_1 - C_{12} \cdot V_2 - C_{13} \cdot V_3 - C_{14} \cdot V_4 \end{aligned} \tag{2.4}$$

This constitutes the first row of the capacitance matrix as

$$\begin{bmatrix} C_{11} + C_{12} + C_{13} + C_{14} & -C_{12} & -C_{13} & -C_{14} \end{bmatrix} \tag{2.5}$$

and the full matrix for the four conductor system as

$$\begin{bmatrix} \sum_{i=1}^{4} C_{1i} & -C_{12} & -C_{13} & -C_{14} \\ -C_{21} & \sum_{i=1}^{4} C_{2i} & -C_{23} & -C_{24} \\ -C_{31} & -C_{32} & \sum_{i=1}^{4} C_{3i} & -C_{34} \\ -C_{41} & -C_{42} & -C_{43} & \sum_{i=1}^{4} C_{4i} \end{bmatrix} \tag{2.6}$$

This can be extended to a more general set of n conductors according to

$$\begin{bmatrix} \sum_{i=1}^{n} C_{1i} & -C_{12} & \dots & -C_{1n} \\ -C_{21} & \sum_{i=1}^{n} C_{2i} & \dots & -C_{2n} \\ \dots & \dots & \ddots & \dots \\ -C_{n1} & -C_{n2} & \dots & \sum_{i=1}^{n} C_{ni} \end{bmatrix} \tag{2.7}$$

which constitutes the general Maxwell matrix.

2.2.2 Cross Coupling between Pixel Plates

The cross coupling is here defined as the capacitance any pixel plate exhibits towards other pixel plates, as illustrated in figure 2.5. Since pixel plates are in close proximity, this capacitance C_p is expected to be large in relation to C_{true} for thicker stack-ups. This will render capacitive fingerprint sensing very hard to implement if not solved.

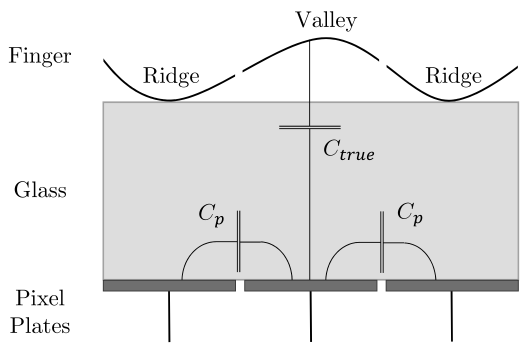

Figure 2.5: Capacitances between neighboring plates often overshadow the capacitive coupling to the finger. Cross-coupling losses are minimized by controlling the potential of nearby plates.

The Maxwell matrix simulations described in section 2.2.1 do define a significant capacitance between plates, however, it is also stated that the induced charge Q on a plate is dependent on the difference in potential V. Therefore, if no voltage change occurs between the plates the capacitance will create no charge difference between them, which is the measured quantity.

2.2.3 Point Spread

A sensor plate does not only couple to its corresponding finger segment straight above the sensor plate, but it also couples to nearby finger segments. This issue becomes more severe as the glass thickness is increased since the relative distance difference between two nearby finger segments diminishes in accordance with the Pythagorean theorem. In figure 2.6 a schematic view of the capacitive couplings in a sensor stack-up is given.

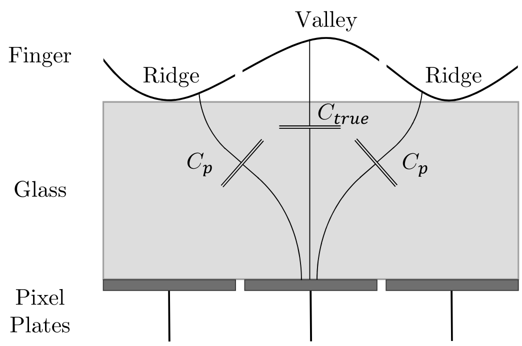

Figure 2.6: Point spread is an increasingly important issue with thicker glass, since the difference in distance between finger segments is reduced in accordance with the Pythagorean theorem.

The point spread is the most prominent effect that equation 2.2 entirely overlooks, resulting in an even smaller difference in capacitance for two nearby plates. In an effort to describe this phenomenon at different stack-up thicknesses a lumped-elements simulation using Maxwell's capacitance matrix has been carried out at thicknesses d_1 , $d_3 = 3 \cdot d_1$ and $d_6 = 6 \cdot d_1$, all at $\varepsilon_r = 7.5$. A set of 19 by 19 pixel plates (50µm x 50µm) are modeled, and corresponding projected finger segments are added. The finger segments all have the same height, contrary to a regular finger. The purpose is to simulate how much of the total capacitance sensed by the center pixel actually comes from the finger segment corresponding to that pixel, and how much is unwanted capacitance from adjacent finger segments. Figure 2.7 describes the relative, cross-sectional capacitance distribution across finger segments in one dimension, with the middle pixel placed at $\Delta x = 0$µm.

The results do not only show the big difference in point spread, but also the immense change in absolute capacitance values between different stack-ups. For thicker stack-ups we notice that the sum of the parasitic capacitances is larger than the desired capacitance of only the finger segment above the plate. It should be noted that the simulation is made in three dimensions and all results are symmetrical in two dimensions around the middle pixel, therefore the sum of parasitic capacitances is larger than just the sum of points at $d \neq 0$ in figure 2.7 which only plots the data in one dimension.

Figure 2.8b and 2.8a displays the same data as figure 2.7 for the d_1 and d_3 simulations

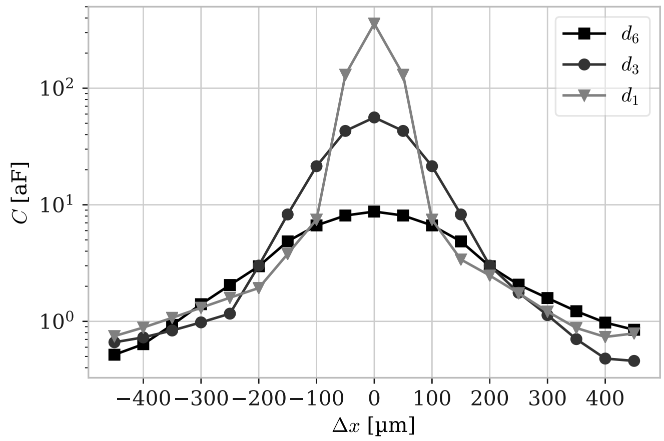

Figure 2.7: Effect of point spread; capacitance distribution is increasingly "smooth" for thicker glass. The effect is prominent; note the log scale.

respectively, but in two dimensions and the values as percentages. One can understand that the point spread will act as an image filter, and only 6.4% of the measured capacitance on a pixel plate can be derived from the finger segment straight above the pixel.

0.0	0.0	0.0	0.0	0.0	0.0	0.0
0.0	0.0	0.0	1.0	0.0	0.0	0.0
0.0	0.0	4.0	10	4.0	0.0	0.0
0.0	1.0	10	33	10	1.0	0.0
0.0	0.0	4.0	10	4.0	0.0	0.0
0.0	0.0	0.0	1.0	0.0	0.0	0.0
0.0	0.0	0.0	0.0	0.0	0.0	0.0

(a) Simulation of a d_1 stack-up with $\varepsilon_r = 7.5$. Each segment represents an area of the finger of the same size as the pixel, 33% of the measured capacitance is related directly to the segment above the pixel.

0.9	0.9	1.2	1.3	1.2	0.9	0.9
0.9	1.2	2.2	2.6	2.2	1.2	0.9
1.2	2.2	3.9	4.8	3.9	2.2	1.2
1.3	2.6	4.8	6.4	4.8	2.6	1.3
1.2	2.2	3.9	4.8	3.9	2.2	1.2
0.9	1.2	2.2	2.6	2.2	1.2	0.9
0.9	0.9	1.2	1.3	1.2	0.9	0.9

(b) The same simulation conducted on a d_3 stack-up, three times as thick as the d_1 stack-up, with $\varepsilon_r = 7.5$. Now only 6.4% of the measured capacitance is related directly to the segment above the pixel.

Figure 2.8: Point-spread functions for two simulated stack-ups: d_1 and d_3, with d_3 being three times as thick as d_1.

2.2.4 Point Spread Described as Low-pass Filter

For those experienced in image processing it might become apparent that figure 2.8a and 2.8b look much like convolution kernels for a discrete, spatial, low-pass filter. Figure 2.9 illustrates the similarities between our simulated point-spread function and a Gaussian low-pass convolution kernel.

0.9	0.9	1.2	1.3	1.2	0.9	0.9
0.9	1.2	2.2	2.6	2.2	1.2	0.9
1.2	2.2	3.9	4.8	3.9	2.2	1.2
1.3	2.6	4.8	6.4	4.8	2.6	1.3
1.2	2.2	3.9	4.8	3.9	2.2	1.2
0.9	1.2	2.2	2.6	2.2	1.2	0.9
0.9	0.9	1.2	1.3	1.2	0.9	0.9

(a) Simulated point-spread function.

0.2	0.5	1.0	1.2	1.0	0.5	0.2
0.5	1.4	2.5	3.0	2.5	1.4	0.5
1.0	2.5	4.4	5.3	4.4	2.5	1.0
1.2	3.0	5.3	6.4	5.3	3.0	1.2
1.0	2.5	4.4	5.3	4.4	2.5	1.0
0.5	1.4	2.5	3.0	2.5	1.4	0.5
0.2	0.5	1.0	1.2	1.0	0.5	0.2

(b) Gaussian low-pass convolution kernel with $\sigma = 1.5969$.

Figure 2.9: Similarities between a simulated point-spread function and a gaussian low-pass filter kernel.

This means that the point-spread effect appears as a blurring of the image, with thicker stack-ups applying more spatial low-pass filtering, i.e. blur. Looking at the spatial frequency response of these two kernels this can be confirmed as described by figure 2.10.

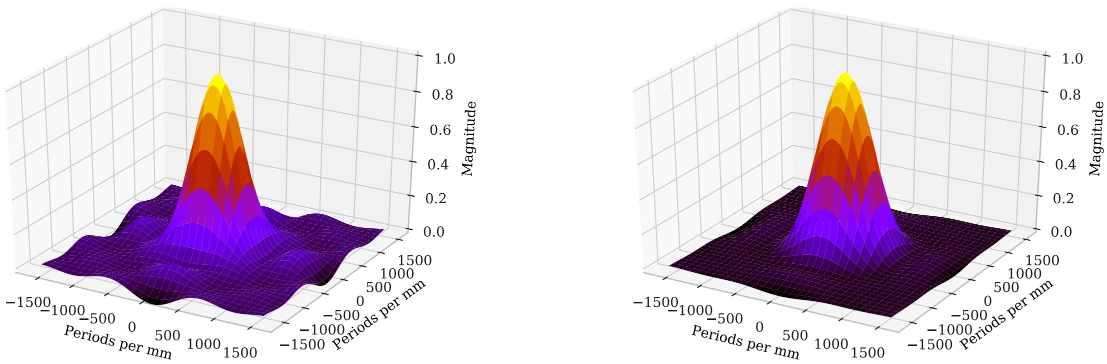

Figure 2.10: The spatial frequency response of two convolution kernels. To the left is the simulated pointspread of a d_3 stack-up, to the right is a Gaussian kernels with sigma $\sigma = 1.5969$.

2.3 Charge Amplifier

The fingerprint sensor circuit is based on the principle of detecting extremely small charges induced by the capacitive coupling between the sensing plate and the finger as described in section 2.1. One way to detect a charge difference is to use a charge amplifier to translate it into a voltage level which later can be amplified and sampled. A generic charge amplifier can be described by the schematic in figure 2.11 and the corresponding model for an ideal circuit is described in equation 2.8.

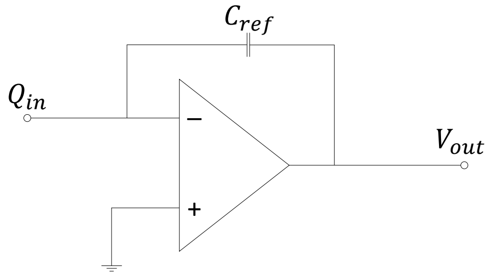

Figure 2.11: A charge amplifier circuit, it can output a voltage V_{out} proportional to the input charge Q_{in}.

$$V_{out} = -\frac{1}{C_{ref}} \cdot Q_{in}[V] \tag{2.8}$$

2.4 SNR

The Signal-To-Noise ratio (SNR) delineates the relation of powers between the signal of interest and the noise. The SNR is described by equation 2.9 [18]. SNR is a telling property since the signal can be drenched by several different noise sources, for example thermal noise as described in section 2.5.1.

$$SNR = 10 \cdot log_{10}\left(\frac{P_{signal}}{P_{noise}}\right) = 20 \cdot log_{10}\left(\frac{A_{signal}}{A_{noise}}\right)[dB] \tag{2.9}$$

2.5 Noise

Since noise can be a limiting factor for biometric performance in a system, it is important to understand what relevant sources of noise exist. In this section we outline the most relevant noise sources and their behavior. Averaging of samples as a method to reduce noise power is also presented.

2.5.1 Thermal Noise

Thermal noise is an approximately white electrical noise that occurs in all circuits due to the thermal agitation of electrons in resistive materials. Thermal noise is also often called *Nyquist-Johnson noise* after its discoverers [19] [20]. The voltage noise from a resistance is described by equation 2.10

$$\Delta V_{noise} = \sqrt{4 \cdot k_B \cdot T \cdot R}\left[\frac{V}{\sqrt{Hz}}\right] \tag{2.10}$$

where k_B is the Boltzmann constant, T is the temperature and R is the resistance [20]. Thermal noise in a capacitive circuit has the same resistive source, but is independent of the resistance magnitude due to higher resistance resulting in both higher generated noise, but also higher filtering of said noise. The thermal noise across a capacitance can be described by equation 2.11 [21], where C is the capacitance.

$$\Delta V_{noise} = \sqrt{\frac{k_B \cdot T}{C}}\left[\frac{V}{\sqrt{Hz}}\right] \tag{2.11}$$

In a sensor design that is highly dependent on small capacitances such as an fingerprint sensor, the thermal noise quickly becomes a problem. Especially since the noise is introduced early in the signal chain, and all subsequent amplification only makes matters worse.

2.5.2 Quantization Noise

In all quantized systems there is some fundamental and unavoidable noise due to the quantization error when converting analog signals to their digital counterpart [18]. The noise power introduced by quantization error is described by equation 2.12 where n represents the number of bits in the ADC, Δ represents the range of one level while R_{ADC} is the range of the ADC [18]. This assumes that all input values within the range of any ADC level are equally probable, which in our case is a good assumption.

$$P_{err} = \frac{\Delta^2}{12} \approx \frac{R_{ADC}^2}{12 \cdot (2^{2 \cdot n})} \tag{2.12}$$

The fingerprint sensor does not provide time-variant signals to sample, resulting in a constant signal for each pixel with some random distribution of noise. This violates the above mentioned conditions; however, the condition still applies when looking at a larger amount of pixels producing multiple different signal levels.

To relate the noise power to the signal power is more complex, since the signal is static. In an ideal case, the power would be similar to that of a full range sine wave, when each ridge reaches the maximum input value of the ADC and each valley reaches the minimum. However, such a perfect signal would be rare in practice and signal powers are expected to be lower, rather than higher.

2.5.3 Noise Averaging

Noise averaging is a signal processing technique that is possible to use on signals that are static. By measuring the same signal multiple times one can reduce the random noise that is obscuring the signal since the noise varies but the signal does not.

The improvement in SNR can ideally be described by equation 2.13 if the following requirements are fulfilled: the noise is random and uncorrelated with the signal, the variance of the noise is constant, the signal is constant and the signal utilizes the full dynamic range of the system [18].

$$SNR_{averaged} = SNR + 3 \cdot \log_2(N)[dB] \tag{2.13}$$

where N is the number of times the signal is sampled.

1

2.6 Necessity of High SNR for Thick Stack-ups

Thicker stack-ups have needs for better SNR for two main reasons:

- Diminishing signals levels
- “Filterability” of point spread

The signal drastically diminishes with distance, as mentioned before, which calls for higher gain levels, aggravating SNR.

Point spread is heavily dependent on stack-up thickness as well, as described in section 2.2, and is significantly more prominent with increased thickness. It is possible to reverse this operation if one finds the frequency-domain inverse or the point-spread kernel. This inverse kernel will become some kind of high-pass filter and will, in ideal conditions, restore the image; a process called “deblurring”. The process is an ill-posed problem because of the inherent instability of the filter and it is well known that the success of it is highly dependent on the input SNR [22].

Point spread is an electromagnetic fundamental principle and is applied to the signal before it is sensed by the pixel plates. This means that all noise that is applied, thermal noise and quantization noise alike, is applied after this effect. If one tries to reverse the point-spread effect in the digital domain higher frequencies of the applied noise will get heavily amplified. To mitigate this the inverse filter is made to not be as aggressive, at the cost of accuracy.

Appendix A provides an example of the process of trying to restore an image. An image is captured with relatively low point spread, then the simulated point-spread kernel is applied to the image. A small amount of white, Gaussian noise is added, then the frequency inverse of said point-spread kernel is applied. In theory the resulting image should be similar, if not identical, to the first image. That is however not the case, and the applied noise dominates within the image, with the exception of the main spatial frequency of the ridge-valley structure at period of about 10-15 pixels.

The "filterability" of the point spread, i.e. how accurate the anti-filter can be, has been shown to be dependent on the SNR of the acquired image. It should be mentioned that the accuracy of the inverse filter also depends on the accuracy of the point-spread kernel that was used to create it. This is, however, regarded attainable through detailed simulations and it is the noise that poses the true challenge for this method's effectiveness.

3

System Descriptions and Methods

In this chapter, a description of the hardware used in this project is provided. We detail the system-level architecture of the sensor ASIC as well as its noise performance. Methods for calculating contrast are described, as well as describing our definition of contrast in this context. Methods for specific investigations are also described.

3.1 System Description

In this section a brief, and simplified, system description is presented which is applicable to the systems that our tests and investigations will be performed upon.

The sensor system is built from an array of sensing metal plates, as described in section 1.2, which couples capacitively to the finger. This capacitance is marked C_{finger} in figure 3.1, which describes the signal path of the sensor. Q_1 is then proportional to the capacitance C_{finger}, and V_1 is in turn proportional to Q_1 in accordance with equation 2.8. Configurable analog gain is applied before the signal is sampled and quantized by the ADC. This sampled value becomes the intensity value for a pixel in an acquired image.

3.1.1 Noise Sources in the System

The system is limited by noise when measuring extremely small signals, such as in applications with thick stack-ups. The charge amplifier is the most vulnerable block in the chain, since it is the first conditioning stage for the measured quantity. Since the measured capacitances are so small (aF range) the charge amplifier will have to achieve high amplification. This has two effects: the noise in node Q_1 will be drastically amplified and C_{gain} will be small, maintaining a low capacitance in the node resulting in high thermal noise since the thermal noise is inversely proportional to capacitance, as described by equation 2.11.

Another source of noise is the quantization noise of the ADC which is discussed

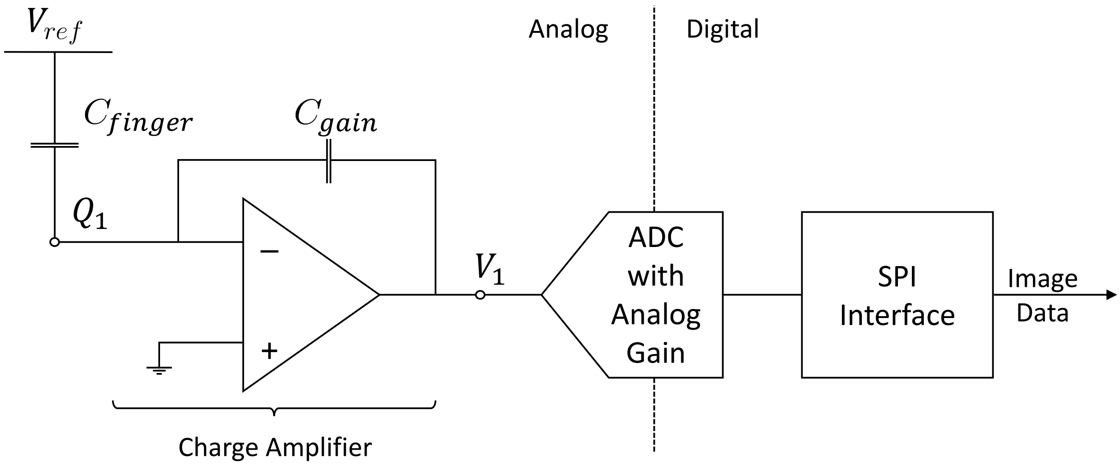

Figure 3.1: A simplified signal path description for the fingerprint sensor.

in the theory chapter. It is difficult to gauge this, since it is dependent on the signal power, but if one assumes a full range sine wave one finds that the SNR equates to $6.02 \cdot 8 + 1.76 = 49.92$ [dB]. This introduces a breaking point in input capacitance where the charge amplifier limits the noise performance, as opposed to the quantization. However, the tested system features noise filtering techniques, which are effective when measuring static signals, increasing SNR by roughly 3dB per doubling of samples [23]. The theoretical maximum SNR, with full analog filtering, before quantization is shown in figure 3.2. Now the breaking point shifts down in capacitance, making the system more robust to lower signal levels and subsequently thicker stack-ups. It turns out that C_{gain} does not affect SNR since it amplifies both the noise and the signal equally; it does however change the operating input range of the charge amplifier. The solid line is a compound of all gain settings to illustrate the entire usable range.

3.1.2 Noise Measurement

In order to evaluate different sensor setups in terms of noise suppression we need to accurately measure the present noise in any given setup. Here, a large number of full images will be collected from the sensor and the standard deviation, annotated as σ, of each pixels value, across all images, will be calculated. The standard deviation is proportional to the square root of the variance, which in turn is proportional of the noise power, namely the noise energy per sample. Therefore we conclude that lower pixel σ will signify better noise performance. It should be noted that the pixel σ will be heavily dependent on system parameters, such as gain, and can only be used comparatively when using identical settings and system architectures.

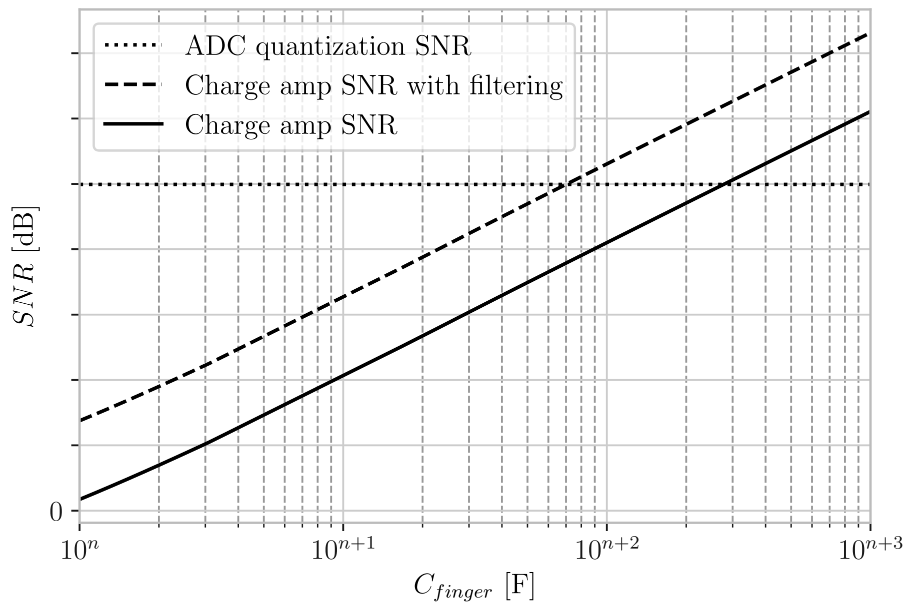

Figure 3.2: Simulated SNR versus input capacitance of a charge amplifier, with and without noise-filtering techniques. A baseline of the quantization noise of the ADC is included to illustrate how the breaking points shift when introducing noise filtering.

3.2 Contrast Definition

We have earlier introduced contrast as a metric. In this section we aim to explain how we define and measure contrast. Contrast is the average difference in ADC-code between ridges and valleys in a certain area, often an entire image. To obtain the contrast for an entire image a large set of pixel locations, marked with either 'peak' or a 'valley' flag, is defined. These are in practice found with an algorithm described in section 3.2.1. The arithmetic mean of the contrast for the image is then calculated based on these points according to

$$ct_f = \frac{1}{n}\sum_{i=1}^{n} r_i - \frac{1}{m}\sum_{i=1}^{m} v_i \quad [1] \tag{3.1}$$

where n and m is the number of ridge and valley coordinates found in the picture respectively, r_i is the ADC-code at the top of a ridge and v_i is the ADC-code at the bottom of a neighboring valley. This renders a single numeric value for each captured image which can be used as a quality indicator; we call this ct_f.

This enables us to study the course of events with a corresponding quality measurement for each image during a finger touchdown.

3.2.1 Contrast Calculation Algorithm

The multi stage process used to find the ridge and valley locations starts by obtaining the raw data array of a picture and forming it to a two-dimensional gray scale image of the fingerprint. A mask is then applied to the image to mark the valid area for algorithm detections. This is done based on the mean value of rows and columns to ensure that the finger has actually touched the area of the sensor. The image is then filtered to render a smoothing effect which enables our algorithm to identify the centers of ridges and valleys more easily. A peak detection function is run on each row or column based on the orientation of the fingerprint to detect the coordinates of ridges. The image data is then inverted and the same peak detection function is then ran to detect the coordinates of valleys. The coordinates are then used to calculate ct_f according to section 3.2. The process is then repeated for the next image.

The process described above is also outlined in figure 3.3 where an example image is used for illustration. This process requires some extensive computational power since a recording of a single finger touchdown sequence can consist of thousands of images.

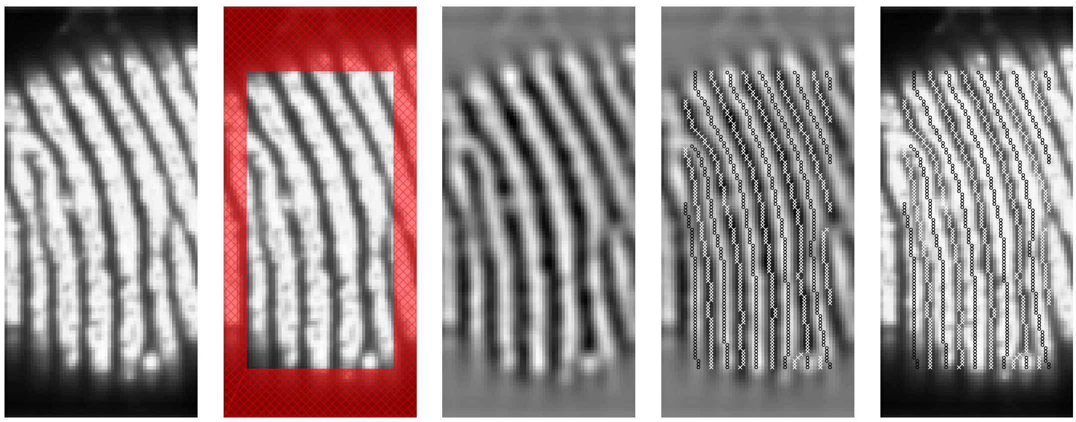

(a) Raw data. **(b)** Mask. **(c)** Filtered image. **(d)** Peak detection to find r_i and v_i coordinates. **(e)** Contrast extraction from raw data.

Figure 3.3: Process to extract contrast from an image. 3.3a shows the raw data before it is masked according to 3.3b and filtered into 3.3c. Peak detection is then run to detect the coordinates of all ridges (black rings) and valley (white crosses) as seen in 3.3d before the contrast can be extracted from 3.3e.

3.3 Multisampling as Noise Supression

According to section 2.5.3 there is a possibility to reduce noise by sampling the same signal multiple times and making the output the average of all samples. In our context of ASIC sensors there are three ways of doing this: analog, digital on ASIC and digital outside ASIC. The locations of these are described in figure 3.4. We would like to compare different analog and digital multisampling implementations both in the ASIC and in post-processing since the ASIC implementation of both analog and digital multisampling might differ from theory and the noise added by the ADC is in practice unknown. To achieve this, a large number of images will be collected for each setup, with a static image in the form of a rubber stamp clamped with constant pressure on the sensor. From this data the average standard deviance (σ) in pixel value across all pixels, and images collected, will be calculated. The σ is expected to decrease with increased multisampling depth, as noise levels get suppressed, and the different implementations are expected to have similar performance.

Analog multisampling could be done by introducing a number of sample capacitors just before the ADC, inserting the signal into them at different times and then sample all of the capacitors at the same time with the ADC. By configuring the number of the capacitors that should be used one can trade off noise supression for sampling time. Sampling once grants short sampling times but might introduce severe sensitivity towards noise which might render the sample unusable for high gains.

Digital multisampling could be done by sampling and quantizing the signal multiple times with an ADC and then combining the samples in the digital domain. To demonstrate the effect on a sensor without digital multisampling capabilities we will have to read the data from the sensor over the SPI-bus, and then do the combination of samples in software. Doing this in software should compare equally to a potential ASIC implementation.

3.4 Dynamic Stop for Multisampling

The use of deep multisampling rates requires a dynamic rate that aborts acquisition if the measured signal no longer is static, in our case this would happen if the finger moves in the parallel direction to the sensor when doing multisampling. A set of small experiments was conducted with 45 frames of digital multisampling, and some analog filtering, fully utilizing our given time frame to maximize noise performance but now without using the dynamic stop condition. When moving the finger heavy distortion occurred and all samples were virtually unusable for authentication. Figure 3.5 shows an image acquired during this investigation. We believe that this is sufficient basis to conclude that the rate of failure of authentication would be unacceptable for multisampling rates this deep without using the dynamic stop condition as a safe

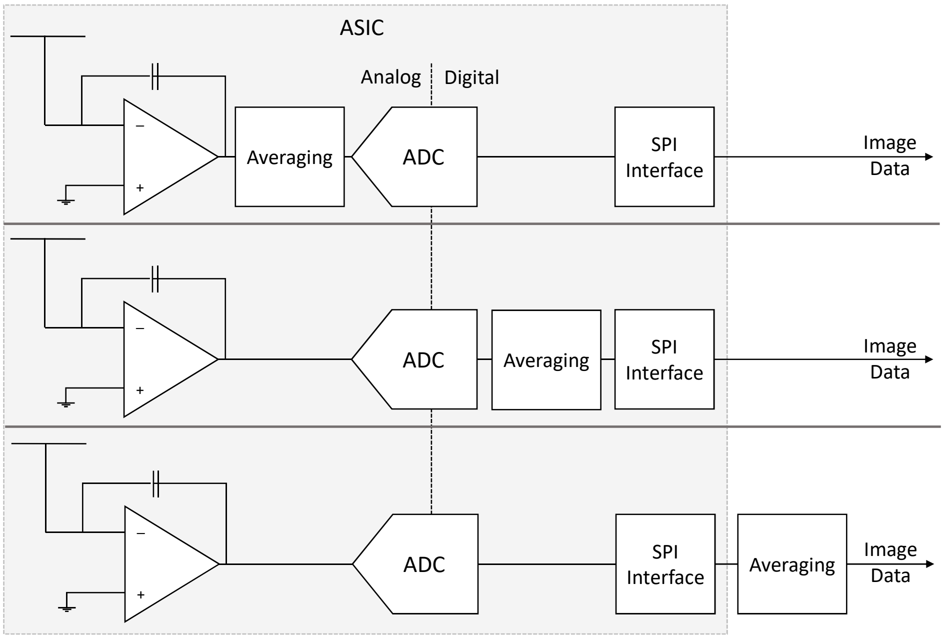

Figure 3.4: Three different techniques to test averaging, Analog, digital on ASIC, and digital averaging carried out by post-processing the data.

guard.

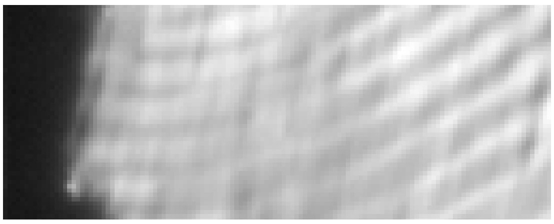

Figure 3.5: A capture with a digital multisampling depth of 45 frames, and analog depth of 4 samples, of a moving finger without using the dynamic stop condition. Image is heavily distorted and thus unusable.

4

Results

All results are presented in this chapter. First we introduce the outcome of the investigation of contrast over time during a finger touchdown sequence. In the latter part of this chapter we delve deeper into noise suppression through both analog and digital multisampling. At the end we show some results based on adding a dynamic stop for the digital multisampling.

4.1 Contrast Data

An extensive data collection has been conducted to characterize contrast behavior over time. Twenty captures for all fingers on both hands were collected for two individuals. One capture comprises about 800 full images. Absolute time is confidential but a normalized time scale is presented with $t = 100\%$ being less than one second from $t = 0\%$, the touchdown moment. The time when $0\% < t < 20\%$ represents the most interesting time frame to capture an image due to end user and customer requests. Three different stack-ups were used. Their absolute thicknesses are confidential but their relative thickness are: $d_1 = d$, $d_2 = 2.4 \cdot d$, and $d_5 = 4.2 \cdot d$.

Since the data set is large, mainly statistical models will be used in presentation as to avoid cluttered plots with many lines. Shown metrics will be arithmetic mean, mode, and standard deviation, σ. All data will also be normalized, since absolute contrast values are not of interest but rather their time behavior. Contrast seems to settle at a certain value after a certain time, therefore the maximum value of the end of the sequence was used as the 100% level. Figure 4.1 shows the specified metrics metrics for all collected captures.

Little time variation is observed in the mean value, with slightly lower contrast early in the sequence, contrary to our hypothesis. The most noteworthy property of this graph is the σ level; contrast is exceptionally uncertain at early times. This is also the point in time where the mode exceeds the mean the most, meaning that the distribution of contrast is skewed towards higher values. This could indicate that contrast peaks do occur in this time frame but are weighed down by captures with

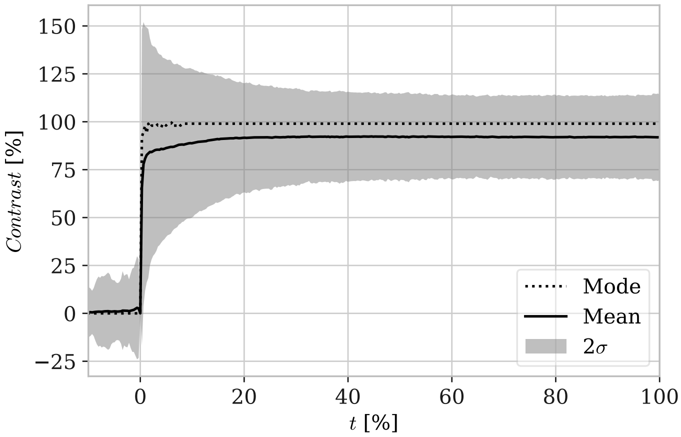

Figure 4.1: Contrast over time for all captured sequences with different fingers, persons and stack-ups. No clear behavior with regards to time is identified in the contrast magnitude. Uncertainties are also high as the large σ illustrates. Data set consists of 1200 captures.

bad contrast. Looking further at smaller data sets this can be confirmed; figure 4.2a shows a set of capture on one person's little fingers on the d_1 stack-up. However, a peak of this strength is only observed in this specific data set. Other little fingers might not share the same behavior, as observed already in this small data set with only two individuals. Even the same person's little fingers might not behave the same on another stack-up as described by figure 4.2b.

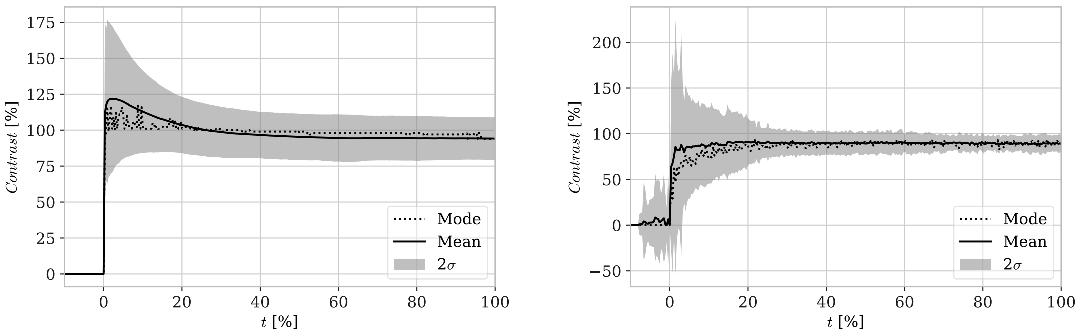

(a) Stack-up with thickness d_1: a clear peak in contrast can be observed.

(b) Stack-up with thickness d_5: the same peak cannot be observed

Figure 4.2: Contrast over time for one person's little fingers on two stack-ups: d_1 and d_5, with 40 captures for each.

Going further the opposite behavior is prevalent with the, normally, most used fingers when authenticating on a phone: index fingers and thumbs. Figure 4.3 shows that for both the d_5 and d_1 stack-ups, the mean value does not have any peak early and that it does not reach its maximum value until after some time. This makes it difficult to determine if taking an image at a specific time can be beneficial. For some specific cases it can be fruitful, but for other cases it might be deteriorative, as seen in the dominant peak in figure 4.2a and the lack thereof in figure 4.3b.

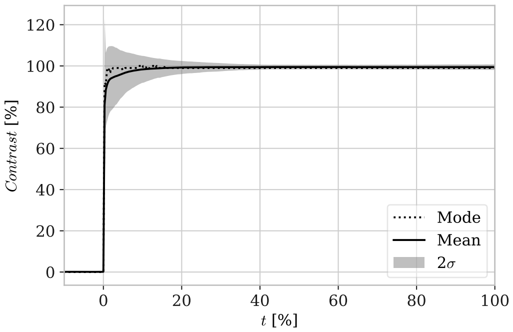

(a) Stack-up with thickness d_1: contrast is low or uncertain at $t < 20\%$

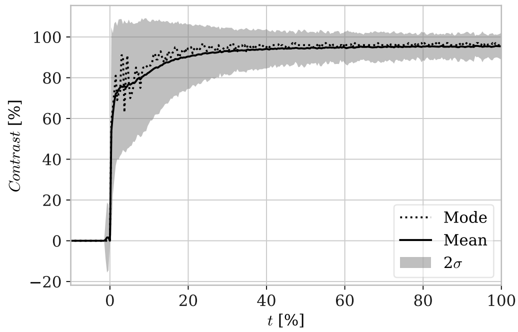

(b) Stack-up with thickness d_5: the same behavior is observed, but stronger.

Figure 4.3: Contrast over time for one person's index fingers and thumbs on two stack-ups: d_1 and d_5, each with 80 captures.

4.2 Multisampling Investigation

The methods described in section 3.3 have been used to investigate the noise of the entire signal chain for two different sensors with different capabilities. In this section we present the results from two different sensor generations.

4.2.1 Analog vs Digital Multisampling

We have performed measurements of the noise performance of the most recent sensor design from FPC. The sensor design includes a number of possibilities to do analog averaging over different sampling capacitors along with extensive possibilities to control the timing and voltage references of the sampling setup. We have compared this analog averaging with digital averaging according to the methods described in section 3.3. The results are presented in figure 4.4.

4.2.2 Location of Digital Multisampling

An ASIC system available at FPC utilized extensive digital averaging, and we put this design to the test by performing noise measurements. The digital averaging inside the ASIC is evaluated against averaging in software, according to section 3.3. All results point to that the methods are identical in noise performance, if the results from averaging in software are quantized back to the same bit depth as the ASIC outputs, which is to be expected since their fundamental operations are virtually identical.

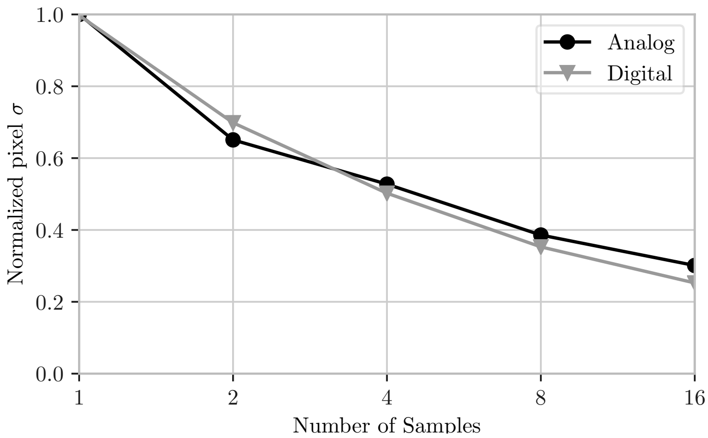

Figure 4.4: Noise performance of Analog and Digital multisampling. Results are similar, with the digital multisampling method following the theoretical performance more closely.

4.2.3 Dynamic Multisampling Rate

A potential vulnerability of any kind of multisampling is sample uncorrelation; if the vast majority of the acquired samples do not contribute to the desired signal their running sum may be degraded instead of strengthened. This means, in the context of fingerprint images, that one is sensitive to finger movement during image capture. If the ridge and valley structure moves perpendicular to its direction there is risk that the addition of more samples will destroy the ridge and valley patterns in the running sum, as described by figure 4.5.

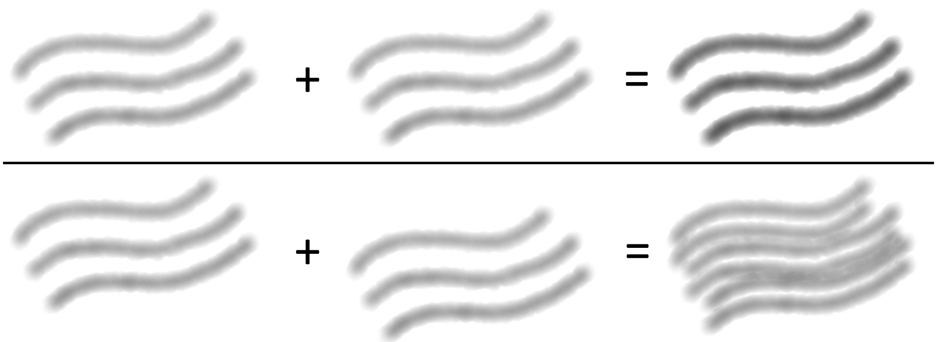

Figure 4.5: Top: a successful correlation, samples are contributing to the pattern. Bottom: an unsuccessful correlation, the addition of the second sample destroys the pattern.

Our proposal to guard against potential degradation is to introduce a dynamic multisampling rate, one which stops if it detects any movement. A conceptual description of this block can be found in figure 4.6. Within the ASIC an image subset is saved and compared with the next image subset. If their difference does not exceed a limit, g, the process continues and a new image is requested. Full image data is in this process sent to a host, outside of the ASIC, which is in charge of adding all incoming data. When receiving notice that movement has occurred the running sum should be stopped, and the result be divided with the number of images gathered, k.

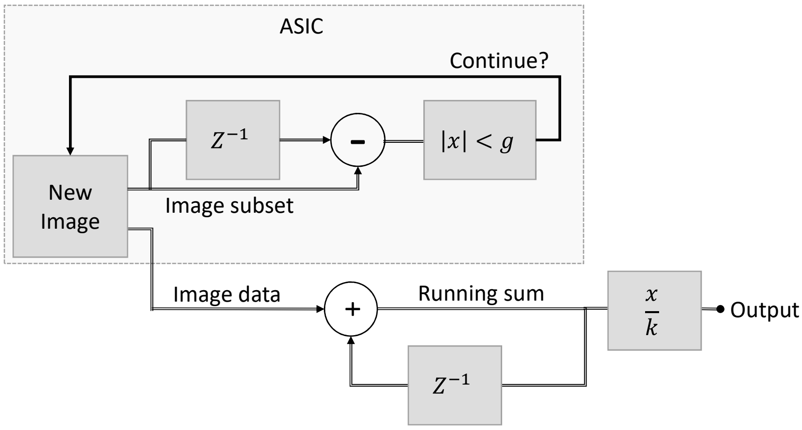

Figure 4.6: Functional block diagram of a dynamic multisampling implementation. For each iteration k, a new image is requested. The difference between the current and last frame is compared to a threshold g which acts as a stop condition for the accumulating sum.

This block was implemented as a prototype in software. We continuously read image data from the sensor, correlating the image subsets from gathered images in parallel, until a stop condition is met. Testing shows that the sensor is able to capture images indefinitely, but in a real case there would be a constraint about how long time it takes to authenticate a user. This constraint limits us to about 45 images given current sensor architecture, specific timing setup, and the time requirements in place at FPC. This results in superior noise suppression as described by figure 4.7, where the normalized standard deviance σ is plotted for different multisampling depths. We surpass the current sensor achitecture's best case noise performance by cutting the pixel value standard deviance in half. It should be noted that the presented numbers of samples are digital only and that the timing settings allow for some analog multisampling as well, improving our results. For comparison a line is plotted with the measured noise performance of the full depth analog multisampling in gray.

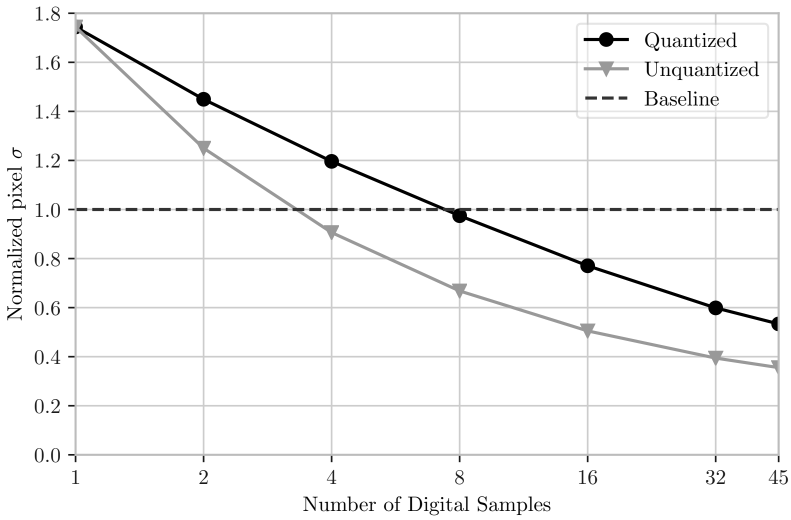

Figure 4.7: Noise averaging performance, plotted as multisampling depth against normalized pixel standard deviance. Both results with and without quantizing the averaged samples back to the output bit depth are presented, as well as a baseline which represents the best case noise suppression with full analog multisampling.

5

Discussion

In this chapter we will discuss the results from chapter 4 with respect to the theory and methods presented in chapter 2 and 3 respectively. First, we discuss the results on contrast in section 5.1 and 5.2. Secondly, we discuss the motivation for improving SNR in section 2.6. Then, in section 5.4 and 5.3 we discuss the multisampling techniques and their implications on implementations. At the end of this chapter we look into some additional experiments that were performed and in section 5.6 we take a holistic view on the ethics of biometrics and their use in society.

5.1 Contrast over Time

Section 4.1 displays and comments on the contrast data that has been gathered. Here, we would like to discuss the methods and results used in the contrast over time investigation. Most importantly, it should be noted that the algorithm to extract ridges and valleys described in section 3.2.1 is constructed by us only for the purpose of this thesis. There exist many algorithms for fingerprint detection, many of them are probably both more accurate and require less resource demanding than ours.

The data set used for the investigation is also fairly limited since it based only on two European males. However, by using all fingers available some of the most common diversifications of fingerprints such as pitch, depth, sweatiness, and skin hardness were included. Since the conclusion that the contrast data was too varied, even though we only used this small data set, could be drawn early in the process we did not see the need to further extend the data set.

5.2 Contrast in Fingerprint Periphery

In section 1.4 we described a hypothesis that a fingerprint would contain more information at the fringes of the finger due to less pressure and deformation. In figure 5.1 a typical image from a capture sequence is shown. The image is captured during the finger-press-down sequence, and despite using thick glass and high gain levels no additional data can be found at the fringes of the fingerprint in comparison to the center. One can observe that the distinction between ridges and valleys is weaker at the fringes and that the signal levels are somewhat varied, with saturation at some spots. Additionally, the method of combining data at the fringes of different images had already been investigated by the FPC and also covered by a patent [24].

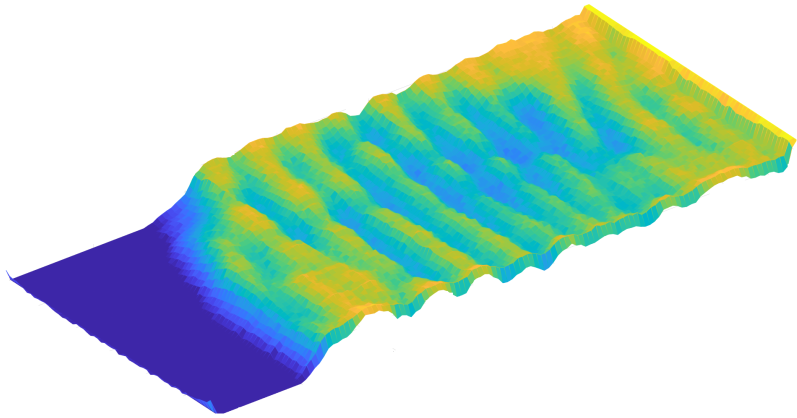

Figure 5.1: The fringes of the fingerprint contain less information than the center despite being less compressed, this is due to the low ϵ_r of air and not fully contacting the glass.

Our thoughts on why the hypothesis proved wrong is based on the fact that capacitive sensing is heavily based on how well the finger is connected to the stack-up. By not having full pressure at the periphery of the finger might render bad contact and a thin layer of air or dirt could act as an insulator, making distinguishment of ridge and valley much harder at the periphery of the finger.

5.3 Location of Averaging

In section 3.3 we described three different ways to do averaging, namely: analog on ASIC, digital on ASIC and digital on host. These methods could also be seen in figure 3.4. In this chapter we aim to discuss the methods with respect to the goals described in section 1.4.

5.3.1 Analog on ASIC

The analog averaging on ASIC is implemented in an available sensor architecture. Therefore, introducing more capacitors and sampling sequences should be fairly easy for analog designers. Analog averaging will however require silicon area, a rare resource in times of price pressure in the fingerprint sensor market segment. The area requirement for analog averaging on ASIC also scales poorly with increased performance, since a doubling of the averaging would require double the capacitive area i.e. linearly.

5.3.2 Digital on ASIC

Digital averaging on ASIC level has also already been implemented in sensor designs. By utilising design blocks as a framework to build upon one can reduce the design effort and NRE costs to design digital averaging. The digital averaging does not require that much area, and most importantly it might scale well with more averages depending on the implementation. The one drawback with doing digital averaging on the ASIC is that it will require some sort of memory for a full image capture, alternatively a smaller buffer but with the risk of being able to capture only a section of the finger before having to abort prematurely if one were to implement the dynamic multisampling scheme, as proposed in section 5.4. A way to address the memory issue is abandon the dynamic multisampling scheme and move to a small number of averaged samples on an image subset, before moving to the next subset. By doing this with a faster sampling sequence one can keep today's time constraints.

Full Image Memory

The most straightforward way of storing data is to store the full image on the ASIC, this would enable the system to continuously capture full images and perform dynamic multisampling as described in section 4.2.3. By storing data we also become more independent from the host, there is no need to wait for I/O-resources or time slots which would reduce the speed and subsequently the performance of the multisampling due to fewer samples.

Sub-image Memory

By compromising with the dynamic multisampling rate one can reduce the area required on the sensor. An additional advantage of using a memory configuration with sub-images is that it can require fewer ADCs if one uses pipelining. Static multisampling can be performed by sampling sub-images multiple times, performing the averaging division and then feeding the data to the SPI-bus before moving to the next sub-image. These sub-images can be as small a single pixel, or as big as a half image. This solution requires the designer to set a fixed number of samples to perform averaging upon. It also has no way of stopping dynamically, which might render the sample unusable if the finger moves during the sampling sequence.

5.3.3 Digital on Host

Digital averaging on the host scales well since it does not require any additional area on the ASIC. Fewer design elements on the ASIC also reduces design and verification costs, as well as power consumption and cost of the ASIC itself. However, some major drawbacks do exist that will render this solution hard to implement in reality; these are mostly related to the data transfer bandwidth from the ASIC to the host. Firstly, the operating system on most hosts are not controlled by FPC, since they are not real time systems we cannot be guaranteed a time slot with enough I/O-capabilities to transfer the required data. Secondly, transferring the raw data to a host is also an inefficient way of utilising the I/O bandwidth since one would need to transfer two full images ($2 \cdot 8 = 16$ bits) instead of sending the addition of the two, which would require, at most, 9 bits.

5.4 Dynamic Multisampling and Time Frame

While the proposed dynamic multisampling scheme has proven to be effective in suppressing noise, its usefulness does rely on a number of assumptions. Here follows a discussion about what might be limiting factors in today's architecture and what might be possible in the future.

We mentioned that the dynamic multisampling scheme is limited to 45 frames, given a time-to-user-authentication requirement. If this requirement were to be relaxed then even more frames could be gathered, subsequently increasing performance. A possible feature of an implementation of this scheme is that it will be easier to change the maximum number of frames; it is just one parameter or register value. This allows for user customisation with a trade off between time to authentication versus biometric performance. This could for example dynamically enable builds of thicker stack-up, or noisier conditions in general, at the sacrifice of speed.

Furthermore, while the 45 frames are limited by time requirements it is also limited by the read-out speed of the sensor. Being built for a static multisampling depth, and not a dynamic continuous capture, the sensor is unoptimized in these working conditions. Introducing a few features, such as more widely controllable internal oscillators, or the option to use external sources, and higher charge amplifier drive strength, could increase the effective frame rate, giving us more than 45 frames in the same time slot.

The location of the averaging, be it on or outside the ASIC, also plays a big part in the effective frame rate. If each frame needs to be sent to a host for storage and processing the overhead, as well as bandwidth, of the communication interface can be limiting. Given that all our testing is done on solutions outside the ASIC it is hard to gauge any potential performance gains.

The analysis of the communication overhead is especially hard since it is asynchronous in relation to the internal oscillators and therefore the entire sampling sequence, and closely matching their bandwidths is a difficult task given the relatively extreme conditions we put the sensor under in order to maximize its output. However, we do expect relatively large gains in frame rate if we were to move the multisampling into the ASIC since any and all overhead of this kind could be eliminated with the two block running on the same clocks.

5.4.1 Mix of Analog and Digital Multisampling

In the results section for the dynamic multisampling rate, and namely in relation to figure 4.7, we mention that analog multisampling is used as well, since timing allows it. This sections aims to clarify why that is and what could be further investigated.

The use of analog multisampling increases read-out times which would decrease the number of frames we could gather in a given time frame in a digital multisampling scheme. We have shown that analog and digital multisampling have similar performance in terms of noise suppression and number of samples. If the time required to take a sample in the analog domain is similar to that of the digital domain it should not matter where the multisampling is done. Given this, it might be unclear why we settled on specifically four analog samples. The reason for this is that our achievable frame rate did not increase according to expectation if we decreased the number of analog samples below four. The conclusion of this being that there exists some overhead, outside the analog domain, which becomes more prominent with short sampling sequences. Where this overhead originates from was only speculated, and not fully investigated, but we do know that the SPI-bus had a hard limit in frequency (thus also bandwidth) due to parasitic capacitances in the transmission lines in our lab setup; this became prominent when trying to use only one analog sample. There should also exist some propagation delay in the digital domain on the ASIC, which might not be optimized for this kind of operation.

In conclusion, if this scheme were to be implemented one must understand why analog and digital samples are not interchangeable, as they would be in theory. This becomes especially important if a digital on ASIC solution is proposed, since any overheads in communication could mistakenly be accounted for.

5.5 Multisampling with Non-identical Samples

In an effort to further increase performance of multisampling we investigated if combination of images taken under different conditions could yield more information. This was in part inspired by the image combining in modern smartphone cameras. The different conditions were in this case different voltage references in the analog domain which resulted in an offset of the entire image. With higher gains and different offsets multiple images could be combined to increase the dynamic range. However, we were not able to achieve anything that surpassed regular multisampling, or increasing the ADC-range or bit depth.

5.6 Ethics in Biometric Identification

Biometric technology has been used for a long time as a means of identification. It used to be based on physical appearance but has during the last few decades increasingly been centred around DNA and fingerprints. The advancement in computing power, electronic devices and sensors has revolutionized the way one can use biometrics to track and identify individuals in society in the last few years.

Biometrics can be used to track people's movements more easily; the most famous examples are surveillance cameras in London and China. Both of these systems are able to use facial recognition as biometric identification to some extent and therefore track suspected criminals. However, the effectiveness of camera based surveillance systems has been questioned [25]. The insight in how these systems are used is due to obvious reasons limited. However, one can easily say that there are ways to perform unethical actions with these systems, such as tracking non-suspects.

Since biometrics are closely tied to the physical appearance there is also a risk of discrimination based on ethnical group, age, or physical abilities [26]. There have been reports on technologies that have different biometric performance based on parameters such as those mentioned above [27]. In this thesis we have seen that point spread is severely affecting thick stack-ups, this would render performance issues for people with narrow pitch fingerprints.

A key aspect of using biometrics is that they are per definition hard to change, one cannot in a simple way change the fingerprint or blood composition of a person. This means that great care must be taken into account when working with safety of personal data; if a fingerprint where to be compromised and leaked to the public an impostor might be able to access systems before the user could be removed from the system. One can compare this with using the same password on all websites; if one is to be hacked it might not be possible to change or even know that your biometric data has been compromised. Multiple techniques are used by the entire value chain of actors involved in biometric authentication, but no chain is stronger than its weakest link. Even if the sensor might be able to easily determine when someone is using a fraudulent finger and declare it as a spoof, an unencrypted data link might serve the full purpose for an impostor.

5.7 Adherence to Time-plan

During the first 10 weeks the plan worked well, much thanks to preparatory work done during the autumn such as ordering of computers, hardware, software, and desks. We had a significant change of scope when the contrast data proved to have little usability in this thesis, and our time-plan subsequently went through a lot of changes even though the framework of tasks remained. We feel that we would like to encourage an early start of thesis work, we gained a lot of momentum in the first sprint by not having to start with administrative tasks.

6

Conclusion

This section will summarize the design proposal for an ASIC design that will increase performance with respect to the challenges and goals stated in section 1.4 based on the results in chapter 4.

6.1 Contrast

We set out with the goal to find an optimal timing for image capture. The result showed that there was indeed some change in the contrast with respect to time, but the behaviour was both unpredictable and varied. Despite having a small sample set of only two persons the behaviour showed little to no correlation. Given this we concluded that an increased sample set would not produce any significant results and should only be used to confirm an already observed pattern, not trying to find one. Therefore our goal regarding contrast over time was not met, and we had no valuable results to base an ASIC design upon. The question formulation itself might seem somewhat naive in retrospect, with many unknown parameters and the expectation to find positive results.

6.2 Noise

With the contrast investigation being inconclusive we changed our scope to instead reduce noise as a means to improve SNR. In section 4.2 we concluded that charge amplifier noise is affecting the system more than the quantization noise when using the sensor under thick glass. Our proposal to combat this is to implement digital averaging on the ASIC with a dynamic stop. By doing digital averaging on the ASIC one can implement a dynamic stop with the help of digital correlation, save I/O-resources, gain a significant speed-up and subsequently more samples to average and further increased noise reduction performance. A prototype of this digital multisampling has been tested, and the performance with respect to the time constraints on the sensor is good compared to sensors available on the market.

6.3 Future Research

There are many aspects of fingerprint behaviour that are unknown, especially with respect to how capacitive sensors translate characteristics such as bad contact, pressure, moist and dirt into signal levels. Therefore, research directed more towards the finger and less into ASIC system design may be able draw different conclusions from the fast-capture process. Additionally, to implement our proposed noise reduction solution one would have to consider many more real-world aspects than have been covered by this thesis.

Bibliography

[1] Fingerprint Cards AB, "the market - fingerprints corporate," 2018. *Available at:* `https://corporate.fingerprints.com/en/about-fpc/the-market/`.

[2] D. Maltoni, D. Maio, A. Jain, and S. Prabhakar, *Handbook of fingerprint recognition*. Springer Science & Business Media, 2009.

[3] A. El-Saba, S. Alsharif, and R. Jagapathi, "Accurate, fast, and secure biometric fingerprint recognition system utilizing sensor fusion of fingerprint patterns," in *SPIE Defense, Security, and Sensing*, pp. 80550K–80550K, International Society for Optics and Photonics, 2011.

[4] e. Tsutomu Matsumoto, "Impact of artificial "gummy" fingers on fingerprint systems," vol. 4677, pp. 4677 – 4677 – 15, 2002.

[5] P. Moorhead, *Qualcomm's New Fingerprint Sensors Go Through Metal, Glass And Displays*. 2017. *Available at:* `https://www.forbes.com/sites/patrickmoorhead/2017/06/27/qualcomms-new-fingerprint/-sensors-go-through-metal-glass-and-displays/#2dd6a8f81ee1`.

[6] AGC Asahi Glass, *AGC Asahi Glass's New Smartphone Cover Glass Enables Fingerprint Scans*. 2016. *Available at:* `https://www.businesswire.com/news/home/20160223005780/en/AGC-Asahi-Glasss-New-Smartphone-Cover-Glass`.

[7] S. Richmond, "Do fingerprint ridges and characteristics within ridges change with pressure?," 2004. Australian Federal Police - Forensic Services.

[8] ISO, Geneva, "Information technology - Biometric data interchange formats - Part 4: Finger image data," 2011. ISO-19794-4:2011.

[9] FBI, U.S. Government, "Electronic Fingerprint Transmission Specification," 2005. EFTS v7.1.

[10] "FPC1320 / FPC1321 - Product specification," 2017. *Available at:* `https://www.fingerprints.com/build/assets/downloads/fingerprints-fpc-1300-series-product-sheet.pdf`.

[11] Corning Incorporated, *Corning® Gorilla® Glass 5 - Product information*, 07 2016. *Available at:* `https://www.corning.com/microsites/csm/gorillaglass/PI_Sheets/Corning_Gorilla_Glass_5_PI_Sheet_RevB.pdf`.

[12] V. Pishchik, E. R. Dobrovinskaya, and L. A. Lytvynov, *Micro and Optoelectronic Materials, Structures, and Systems: Sapphire : Materials, Manufacturing, Applications*. Springer, 2009.

[13] Advanced Optics SCHOTT North America, Inc., *Sapphire for Advanced Imaging, Sensing and Security*, 05 2013. *Available at:* `http://www.us.schott.com/`

d/ advanced_ optics/ c4834f63-9c1c-4de6-8def-2c9be60e324a/ 1 . 2/ schott-sapphire-may-2013-us. pdf .

[14] E. J. Busselaar, "Improved pores detection in fingerprints by applying ring led's (525 nm)," *Optica Applicata*, vol. Vol. 40, nr 4, pp. 843–861, 2010.

[15] H. B. Palmer, "The capacitance of a parallel-plate capacitor by the schwartz-christoffel transformation," *Electrical Engineering*, vol. 56, pp. 363–368, March 1937.

[16] D. K. Cheng, *Field and wave electromagnetics*. Harlow: Pearson Education, second ed., 2014.

[17] E. D. Lorenzo, "The maxwell capacitance matrix," Tech. Rep. WP110301, FastFieldSolvers, march 2011.

[18] F. Maloberti, *Data converters*. Dordrecht, Netherlands: Springer, 2007.

[19] J. B. Johnson, "Thermal agitation of electricity in conductors," *Physical Review*, vol. 32, no. 1, pp. 97–109, 1928.

[20] H. Nyquist, "Thermal agitation of electric charge in conductors," *Physical Review*, vol. 32, no. 1, pp. 110–113, 1928.

[21] R. Sarpeshkar, T. Delbruck, and C. A. Mead, "White noise in mos transistors and resistors," *IEEE Circuits and Devices Magazine*, vol. 9, no. 6, pp. 23–29, 1993.

[22] M. Paul, "Deblurring images: Matrices, spectra and filtering by per christian hansen, james g. nagy, dianne p. o'leary," *International Statistical Review*, vol. 75, no. 2, pp. 253–254.

[23] G. M. Hieftje, "Signal-to-noise enhancement through instrumental techniques. ii. signal averaging, boxcar integration, and correlation techniques," *Analytical Chemistry*, vol. 44, no. 7, pp. 69–78a, 1972.

[24] E. Setterberg and H. Thörnblom, "Method and fingerprint sensing system for forming a fingerprint image," 2015. U.S. Patent 15359014.

[25] P. Fussey, "Observing potentiality in the global city: Surveillance and counterterrorism in london," *International Criminal Justice Review*, vol. 17, no. 3, pp. 171–192, 2007.

[26] J. Wickins, "The ethics of biometrics: the risk of social exclusion from the widespread use of electronic identification," *Science and Engineering Ethics*, vol. 13, no. 1, pp. 45–54, 2007.

[27] UK Passport Service, *Biometrics Enrolment Trial Report*. May 2005. *Available at:* `http : / / www . dematerialisedid . com / PDFs / UKPSBiometrics _ Enrolment_ Trial_ Report. pdf` .

A

Deblurring Example

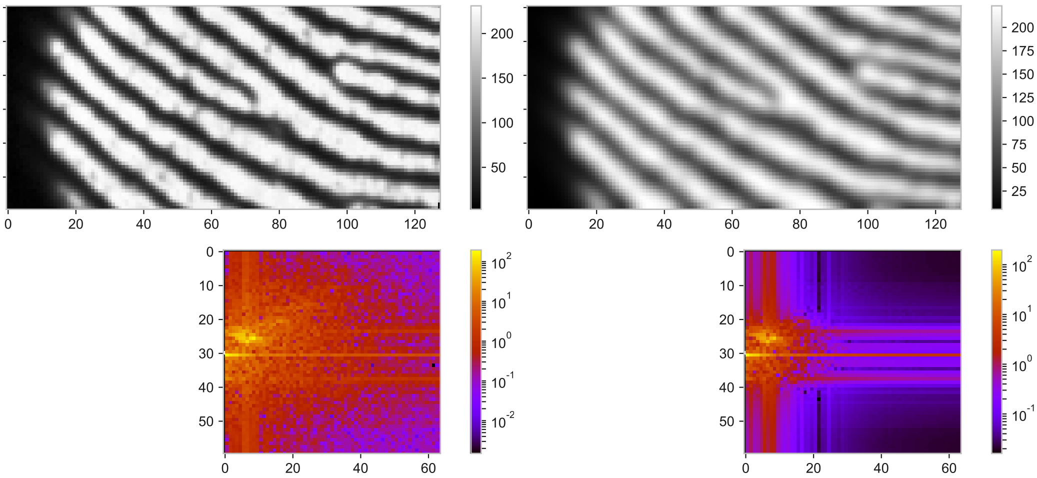

(a) Captured image.

(b) Image digitally filtered with simulated point-spread kernel.

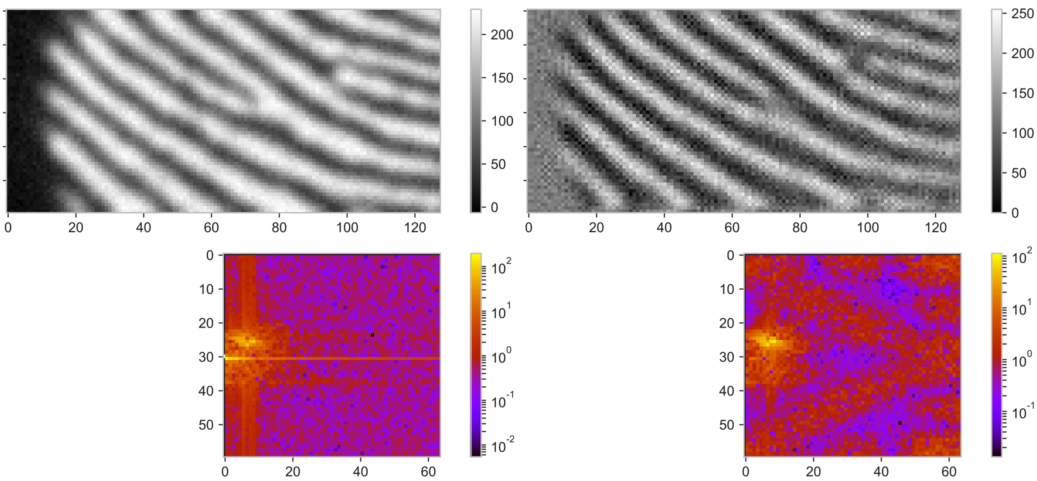

(c) Filtered image with added noise.

(d) Noisy image 'restored' with anti-filter.

Figure A.1: A potential process of trying to restore an image with point spread and analog noise. Images are plotted in each step with its spatial frequency magnitude below.